IEEE
THE INSTITUTE OF ELECTRICAL AND ELECTRONICS ENGINEERS INC.

SIGNAL PROCESSING
ALGORITHMS, ARCHITECTURES, ARRANGEMENTS, AND APPLICATIONS
SPA 2015
September 23-25th, 2015, Poznań, POLAND

Irregular Sampling for X-Ray Imaging Simulation

M. Kröger, M. Rosenbaum, W. Sauer-Greff, R. Urbansky
Institute of Communications Engineering
Technical University of Kaiserslautern,
67653 Kaiserslautern, Germany
Email: mkroeger@rhrk.uni-kl.de

M. Lorang, M. Siegrist
OCS Checkweighers GmbH
Adam-Hoffmann-Str. 26
67657 Kaiserslautern, Germany
Email: markus.lorang@wipotec.com

***Abstract*—The simulation of X-ray images can be computed efficiently using raytracing, a technique well established in 3D computer graphics and rendering. Since raytracing is a discrete technique it is prone to aliasing artefacts. However, irregular sampling is able to mitigate this problem. In this paper the influence of the probability density function of the sampling process on the reconstructed spectral density is described. It is demonstrated that irregular sampling can be used in X-ray imaging simulation to reduce the impact of aliasing.**

I. INTRODUCTION

X-ray imaging simulation is an important step in development between construction and prototyping of X-ray imaging systems. It can be used to estimate the quality of the imaging process and to confirm the geometry of the setup without costly and time-consuming series of tests. This could be achieved by modeling the interactions at subatomic levels. While this would guarantee realistic results, such kind of calculations would be very time consuming. Instead, raytracing uses a more macroscopic approach of interpreting radiation as discrete rays and calculating their interaction with physical properties of materials, like absorption. Since raytracing is a discrete process the effects of sampling and aliasing have to be considered. It is well known that this problem can be mitigated by irregular sampling where the sampling points probability density function (pdf) influences spectral density and noise of the reconstructed images [1].

The remainder of this paper is organized as follows: In Section II the principles of raytracing are described. In addition, the differences between raytracing used for rendering photorealistic images and the application in X-ray simulation are shown. Section III describes sampling, the differences between regular and irregular sampling as well as the impact of using different sample point distribution functions. Finally, in Section IV these effects are demonstrated by some examples and simulated X-ray images rendered with different sampling distributions are depicted.

II. RAYTRACING

Raytracing is a technique for rendering photorealistic images well known in computer graphics. The basic algorithm is based on the idea of emitting rays of light into a 3D scene beginning at the eye point [2]. If an object is hit by a ray, the intensity and color of the corresponding sensor point is calculated depending on the properties of the 3D object. Figure 1 illustrates this basic concept of raytracing.

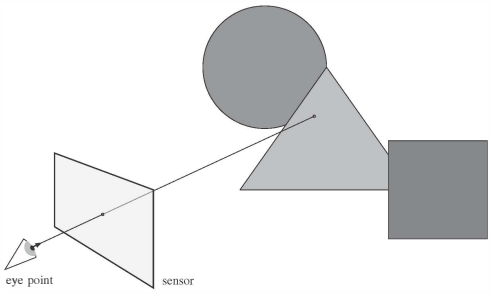

Fig. 1. Schematic of Raytracing

In case of X-ray imaging simulation, the structure differs from the above-mentioned concept. In X-ray laminography [3] the X-ray sensor is contained in a base plate and the X-ray tube is mounted above it. The irradiated volume moves with constant speed through the area between source and sensor as shown in figure 2.

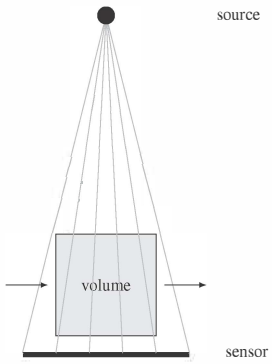

Fig. 2. Raytracing in X-ray imaging

Contrary to the ordinary raytracing, the rays are limited in length between the sensor and the source. In addition, in X-ray imaging the transmission of radiation through the volume and its interaction with materials is evaluated, and for applications

in industrial quality ensurance the objects are large enough to prevent refraction. Initially it is also assumed that there is no scattering in the X-ray propagation. In industrial applications monochromatic X-ray tubes are not used, therefore absorption has to be calculated depending on the photon energy of the X-rays.

The irradiated volume has to be represented in such a way that the path of a ray through different materials can be calculated. One possibility is that the volume consists of homogenous primitives each containing a specific material. These could be simple primitives, e.g. cuboids, bowls, triangles, but also complex forms like Non-Uniform Rational Basis Splines (NURBS). Another way to describe the volume is to model it as a set of finite volume elements (voxel). This, in fact corresponds to breaking down the volume into many very small cuboids consisting of homogenous materials. The latter is much more prone to aliasing than the first.

III. Sampling Distribution Functions

Sampling is the process of converting analog into discrete functions. If a bandlimitted analog function is sampled with a sufficient set of equally spaced points, both representations contain the same information and can be mutually converted. The error which appears due to spectral overlapping when using too less sampling points is called aliasing. By irregular sampling the aliasing artifacts can be replaced by broadband noise which is less visible for human eyes [4]. The following four different sampling point distributions will be considered:

- regular point sampling
- uniformly distributed point sampling
- Poisson-disc sampling
- jittered-grid sampling

The sampling point pdf and its effect on the spectrum of the sampled function will be discussed for the 1D case since it is easier to comprehend these results than in the 2D case.

A. Regular point sampling

Regular point sampling is the well known case of sampling in signal processing. The sampling positions are equally spaced with uniform distance T_A. In this case the sampling function $a(t)$ can be written as

$$a(t) = \sum_{\nu=-\infty}^{\infty} \delta(t - \nu \cdot T_\mathrm{A}) \tag{1}$$

where $\delta(t)$ denotes the Dirac delta function.

The spectrum of the sampling function $A(f)$ can be calculated using the Fourier transform of the sampling function (1):

$$\begin{aligned} A(f) = \mathcal{F}\{a(t)\} =& f_\mathrm{A} \sum_{\mu=-\infty}^{\infty} \delta(f - \mu \cdot f_A), \\ \text{where} \quad & f_A = \frac{1}{T_\mathrm{A}} \end{aligned} \tag{2}$$

Anticipating random sampling, the regular case can be written as a random point process, where the random variable $d_{\Delta t}$ denotes the intervals between sampling points with the pdf $f_{d_{\Delta t}}$. Thus, the regular point sampling process can be described by the pdf

$$f_{d_{\Delta t}}(\Delta t) = \delta(\Delta t - T_\mathrm{A}). \tag{3}$$

Using this consecutive sampling point distances, the absolute sampling points τ_i can be calculated by the sum of previous distances

$$\tau_i = \sum_{\nu=0}^{i} d_{\Delta t,\nu} \tag{4}$$

which can now be used to rewrite the sampling function (1) as

$$a(t) = \sum_{i=-\infty}^{\infty} \delta(t - \tau_i). \tag{5}$$

This form is useful to determine the spectrum of a sample function of this random process by using the Fourier transform and the shifting property of the Dirac delta function:

$$\begin{aligned} \tilde{A}(f) = \mathcal{F}\{a(t)\} &= \int_{-\infty}^{\infty} \sum_{i=-\infty}^{\infty} \delta(t - \tau_i) \cdot \mathrm{e}^{-j2\pi f t} \mathrm{d}t \\ &= \sum_{i=-\infty}^{\infty} \mathrm{e}^{j2\pi f \tau_i} \end{aligned} \tag{6}$$

Figure 3 shows a segment of the regular sampling function and its magnitude spectrum. This magnitude spectrum is calculated according to equation (6) for a finite number of 1000 sampling points. Therefore, such a magnitude spectrum my differ from the theoretical spectrum, e.g. given by (2). However, it can be seen that the periodicity in the time domain also shows up in the frequency domain.

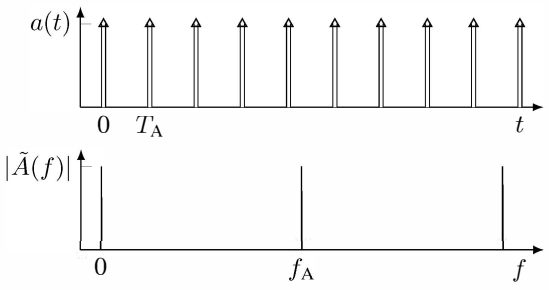

Fig. 3. Segment of the sampling function and magnitude spectrum

From $|\tilde{A}(f)|$ of figure 3 it is obvious that the Nyquist-Shannon sampling theorem states that a bandlimited signal has to be sampled with a sampling frequency at least twice as high as the maximum signal frequency to avoid aliasing.

B. Uniformly distributed point sampling

Uniformly distributed point sampling is a nonregular sampling process with sampling points randomly distributed. This can be described by a point process which generates independent sampling points with an exponential pdf of the point distances [5]:

$$f_{d_{\Delta t}}(\Delta t) = \begin{cases} \lambda \cdot \mathrm{e}^{-\lambda \cdot \Delta t}, & \Delta t \geq 0 \\ 0, & else \end{cases} \tag{7}$$

The rate parameter λ controls how many points are expected per time interval. Since this is a random process it is illustrative to consider a sample function of this process. Figure 4 shows such an example function and its magnitude spectrum.

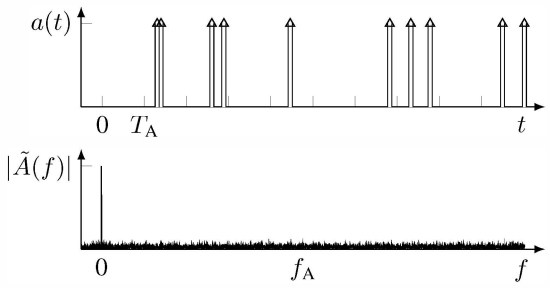

Fig. 4. Segment of an example of the uniformly distributed sampling function and magnitude spectrum

The sampling function shows two conspicuous characteristics: First, there is no regularity in the distribution of the samples. Second, there are some rather large gaps between two points, but also some sample points that are located very close together. This influences the spectrum of the sampling function. It has a DC peak but at all other frequencies there is a noise floor only. Due to the lack of regularity in the sampling function there are no replicas in the spectrum of the sampled signal. Therefore, no aliasing artefacts will be visible, they are replaced by additional broadband noise.

C. Poisson-disc sampling

The basic idea behind Poisson-disc sampling is to prevent the sampling points from getting too close to each other. The use of this sampling point distribution is inspired by the structure of mammal eyes. YELLOT published in 1983 that the extrafoveal cone density in a rhesus monkey retina is smaller than it has to be to satisfy the sampling theorem [6]. But these cones are placed in a Poisson-disc distribution, reducing the visible noise below that expected as a consequence of the violation of the sampling theorem. The minimum distance condition can be achieved by modifying the pdf (7) of the sampling distances:

$$f_{d_{\Delta t}}(\Delta t) = \begin{cases} \lambda \cdot \mathrm{e}^{-\lambda \cdot \Delta t + \lambda \cdot t_0}, & \Delta t \geq t_0 \\ 0, & else \end{cases} \tag{8}$$

Figure 5 shows a sample of the Poission-disc sampling process. In this case the minimum distance of the sampling points is chosen to be three-quarters the regular sampling interval, i.e., $t_0 = 0.75 \cdot T_\mathrm{A}$.

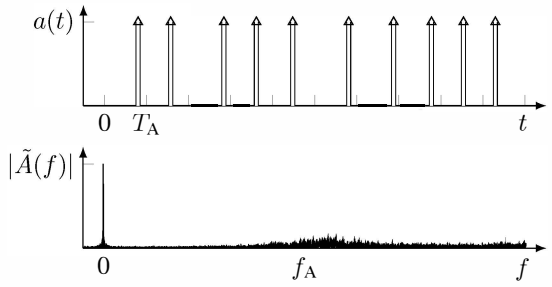

Fig. 5. Segment of a sample function of the Poisson-disc sampling function and magnitude spectrum

As intended the sampling points are not closer than $0.75 \cdot T_\mathrm{A}$. As a consequence the noise floor at low frequencies is low. At high frequencies the noise level is as high as it would be in the uniformly distributed case. This fact predestinates Poisson-disc sampling if it is intended to sample non-bandlimited signals for human eyes, since human eyes are more sensitive to low frequency noise than to high frequency noise. The amount of noise reduction in the low frequency range and the exact appearance of the noise figure changes with the minimum distance t_0. The noise figure varies with the sampling pdf, but the overall noise level does not change [4]. It only depends on the average number of sampling points per unit.

D. Jittered-Grid sampling

The idea behind jittered-grid sampling is to break a regular grid by jittering the sampling positions randomly. The advantage of this approach is the simplicity of calculation. In this case bias free uniformly distributed jitter n_J of the width w is added:

$$\begin{aligned} a(t) &= T_\mathrm{A} \sum_{\nu=-\infty}^{\infty} \delta(t - \nu \cdot T_\mathrm{A} + n_\mathrm{J}) \\ f_{n_\mathrm{J}}(\Delta t) &= \begin{cases} \frac{1}{w} & -\frac{w}{2} \leq \Delta t \leq \frac{w}{2} \\ 0, & else \end{cases} \end{aligned} \tag{9}$$

In figure 6 an example of a jittered-grid sampling function with uniform jitter of width $w = T_\mathrm{A}$ is shown.

The magnitude spectrum of the jittered-grid sampling function shows very low noise at low frequencies but the noise level reaches the uniform noise level at lower frequencies than for Poisson-disc sampling. Interestingly, there will be attenuated peaks at multiples of the sampling frequency if the amount of jitter is too small. This will then cause aliasing artefacts.

It is also possible to use other jitter distributions like normally distributed jitter. They may have other impacts on the spectrum and need to be evaluated in further studies.

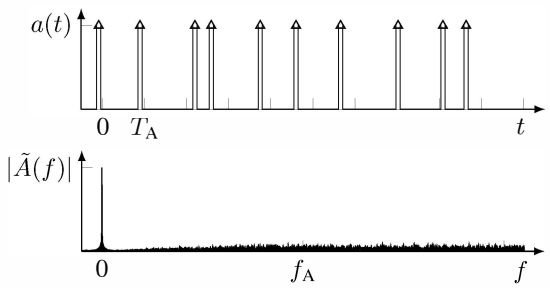

Fig. 6. Segment of an example of the jittered-grid sampling function and magnitude spectrum

IV. Implementation

To compare these four sampling distribution functions they are used in a simple X-ray imaging simulator as shown in figure 2 and implemented in MATLAB. A mono-energetic X-ray point source is assumed which irradiates a volume, consisting of $512 \times 512 \times 512$ voxels. The volume was generated by the function *phantom3d.m* [7].

The target resolution of the sensor is 200×200 pixels. Since the reconstruction of irregularly sampled images is nontrivial, the images are rendered at higher sampling densities and reconstructed by using a multistage box filter as described by Mitchell [8]. The Poisson-disc samples are generated by the function *generate_poisson_2d.m* [9]. At the target minimum distance of $0.75 \cdot T_\mathrm{A}$, where T_A corresponds to the distance of two regular sampling points on the axis, 384343 sampling points are generated which corresponds to an oversampling factor of about 9.6. Correspondingly, the same number of sampling points is applied to uniformly distributed sampling. For regular sampling $620 \times 620 = 384400$ regularly spaced sampling positions are used. For jittered-grid sampling these sampling positions are jittered by the full distance of the sampling points $w = T_\mathrm{A}$.

In this basic simulator a ray only hits one voxel per voxel layer. At flat angles it is possible that a ray can penetrate more than one voxel per layer which could cause additional errors. In the simulator used here the angles of the rays to the central ray are relatively small so this effect can be neglected.

In the consecutive simulated X-ray images are shown rendered using the four different sampling distributions. Figure 7 shows a section of the sensor image using regularly spaced sampling.

In this regularly rendered image prominently visible lines appear. They are due to aliasing effects which can not be suppressed by oversampling and filtering. Apart from that the image containes only little noise.

In figure 8 the sampling points are uniformly distributed.

This picture shows no visible aliasing artefacts. Compared to the regularly sampled image the noise floor is higher. The black pixels are caused by a lack of sampling points in the area of this pixel. Since the sampling positions are uniformly distributed it is not impossible that there are no sampled values within a pixel.

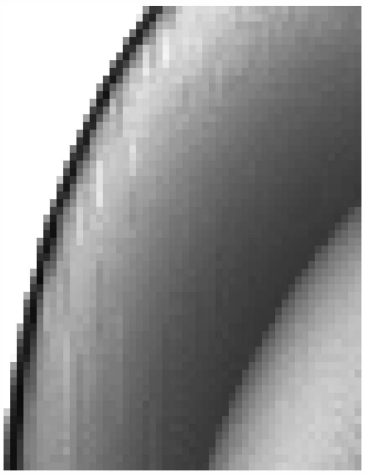

Fig. 7. Phantom rendered with regular sampling

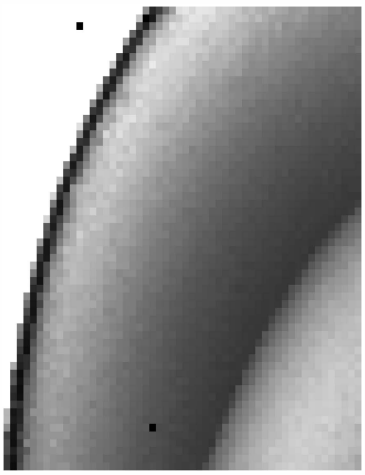

Fig. 8. Phantom rendered with uniformly distributed sampling

Figure 9 shows the same scene rendered with Poisson-disc distributed samples.

In this image neither black pixels nor aliasing artefacts are visible. The noise is also less noticeable compared to uniformly distributed sampling. Because of these properties Poisson-disc sampling is prefered in rendering.

In figure 10 the section rendered with jittered grid sampling is depicted.

Here too, neither visible aliasing effects nor black pixels appear. However, compared to Poisson-disc sampling full distance jittered grid sampling results in an image with more visible noise.

V. Conclusion

Raytracing is an effective way to calculate simulated X-ray images. Aliasing artefacs can be replaced by broadband noise through irregular sampling. This noise can be made less visible for human eyes by Poisson-disc sampling. The reconstruction problem of irregular sampled images is not

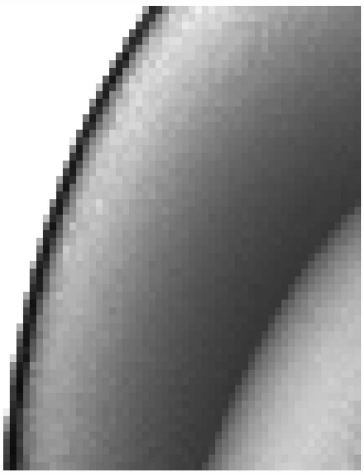

Fig. 9. Phantom rendered with Poisson-disc sampling

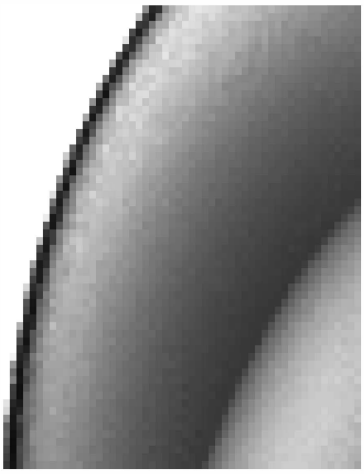

Fig. 10. Phantom rendered with jittered-grid sampling

finally solved. Optimized parameters and sampling pdfs have to be investigated in further studies.

REFERENCES

[1] M. A. Z. Dippé and E. H. Wold, "Antialiasing through stochastic sampling," *SIGGRAPH Comput. Graph.*, vol. 19, no. 3, pp. 69–78, Jul. 1985. [Online]. Available: http://doi.acm.org/10.1145/325165.325182

[2] A. Appel, "Some techniques for shading machine renderings of solids," in *Proceedings of the April 30–May 2, 1968, Spring Joint Computer Conference*, ser. AFIPS '68 (Spring). New York, NY, USA: ACM, 1968, pp. 37–45. [Online]. Available: http://doi.acm.org/10.1145/1468075.1468082

[3] S. Gondrom, S.; Schröpfer, "Digital computed laminography and tomosynthesis - functional priciples and industrial applications," *Preceedings of the International Symposium on Computerized Tomography for Industrial Applications and Image Processing un Radiology*, 1999.

[4] R. L. Cook, "Stochastic sampling in computer graphics," *ACM Trans. Graph.*, vol. 5, no. l, pp. 51–72, Jan. 1986. [Online]. Available: http://doi.acm.org/10.1145/7529.8927

[5] A. Papoulis, *Probability, random variables, and stochastic processes*, ser. McGraw-Hill series in electrical engineering. New York: McGraw-Hill, 1991.

[6] J. Yellott, "Spectral consequences of photoreceptor sampling in the rhesus retina," *Science*, vol. 221, no. 4608, pp. 382–385, 1983.

[7] M. Schabe. 3d shepp-logan phantom. [Online]. Available: http://www.mathworks.com/matlabcentral/fileexchange/9416-3d-shepp-logan-phantom

[8] D. P. Mitchell, "Generating antialiased images at low sampling densities," *SIGGRAPH Comput. Graph.*, vol. 21, no. 4, pp. 65–72, Aug. 1987. [Online]. Available: http://doi.acm.org/10.1145/37402.37410

[9] C. L. Computing. Poisson disc in matlab. The University of Western Ontario. [Online]. Available: http://cusacklabcomputing.blogspot.de/2013/07/poisson-disc-2d-in-matlab.html